Spectral features of Forbush Decrease during Geomagnetic Storms

Rabin Baral[1], Binod Adhikari[1,2] *, Andres Calabia[3], Munawar Shah[4], Luis del Peral[5], María D. Rodríguez Frías[5], Roshan Kumar Mishra[1], Sudarshan Bohara[1], Roshna Manandhar[1]

[1] Department of Physics, St. Xavier's College, Tribhuvan University, Kathmandu, Nepal.

[2] Department of Physics, Patan Multiple College, Tribhuvan University, Nepal.

[3] School of Remote Sensing and Geomatics Engineering, Nanjing University Information Science Technology, China.

[4] Department of Space Sciences, Institute of Space Technology, Islamabad, Pakistan

[5] Space and Astroparticle Group, University of Alcalá, Madrid, Spain.

***Corresponding Author:** binod.adhi@gmail.com**

Abstract

Geomagnetic storms and Forbush decreases (FD) on Earth are primarily caused by coronal mass ejections (CMEs) and stream/corotating interaction regions (SIRs/CIRs) originated in the Sun, which are propagated as a low-energy plasma disturbances through the interplanetary magnetic field (IMF). In this paper, we study the variations of the solar-wind parameters (solar wind velocity, plasma density, and IMF-B_z component) and the Earth's disturbance storm-time index (D_{st}), in relation to cosmic ray flux measurements from 8 neutron monitor stations distributed over Canada, Russia, Finland, and Greenland, during 3 intense geomagnetic storms occurred during the 24^{th} solar cycle (March 16-18, 2015, June 21-23, 2015, and September 7-9, 2017). The wavelet analysis of the Forbush decrease seen in the cosmic ray intensity reveals the clear evolution of the classical two-step process, and with a peak period of approximately 2.1 h. The correlation-delay analyses show a very strong correlation (~0.9) between the relative count rate changes cosmic ray intensity and the indices of solar wind velocity and D_{st}. We obtain similar time-delay responses to the solar wind velocity for all the cases (~4 hours), but large discrepancies are seen for the D_{st} index between the storms. We therefore recommend not using the D_{st} index for predicting Forbush decreases. Finally, we employ the resulting delay-times to parameterize the Forbush decreases in terms of solar wind, and we obtain a predictive model with R^2 parameter of an approximate value of 0.8. Moreover, we observe a possible dependence on solar wind proton density which modulates the magnitude of Forbush decreases under similar solar wind velocity conditions. Our results verify the suitability of using solar wind parameters to predict Forbush decreases in the cosmic ray flux.

Keywords: Forbush Decrease; Geomagnetic Storm; Continuous Wavelet Transform; Correlation; Solar Wind

1. Introduction

Cosmic rays are charged particles (proton, nuclei, relativistic electrons, antiparticles, etc.) outreaching Earth from outside the solar system with energies ranging between 10^8 eV and 10^{20} eV and beyond. Cosmic rays are essential for the dynamics of the Interstellar Medium through ionization and heating of gases (Karttunen et al., 2016; Svensmark, 2006). The incoming flux of cosmic rays at the Earth's upper atmosphere is mainly modulated by the variable solar wind and its embedded Interplanetary Magnetic Field (IMF), which acts as an outward shield of energy to incoming cosmic rays (Ahluwalia, 2003; Ifedili, 2006). The transition of cosmic ray intensity (CRI) is modulated by various solar and interplanetary variables (Usoskin et al., 2008; Belov, 2008). Immense magnetic disturbances outreach the Earth in the form of interplanetary coronal mass ejections (ICMEs) or solar flares, drifting incoming cosmic rays and decreasing their intensity (Cane et al., 1995; Cane, 2000). Such events act as interplanetary shock drivers. CRIs substantially drop with the emergence of these disturbances (Kharayat et al., 2017; Mathpal et al., 2018). Forbush decrease is characterized as the transient decrease in cosmic ray intensity generated by the disturbances in interplanetary conditions originating from coronal mass ejections (CMEs), solar flares, and high-speed solar wind streams and usually last from one to two days (Cane, 1995; Joselyn, 1986; Singh et al., 2008; Kandemir et al., 2002). Although, both FDs and geomagnetic disturbance are manifestations of a given interplanetary disturbance, their magnitudes are not always proportional to each other (Kane, 1977; Singh et al., 2008). FDs are described as a sudden onset often with a complicated time structure that reaches a minimum within a day. They are followed by a more gradual recovery period that can last anywhere from a few days to a few weeks (Cane, 2000; Zhao and Zhang, 2016; Lingri et al., 2016).

Decrease in the cosmic ray count rate was firstly observed by Forbush (1937, 1938), Hess and Demmelmair (1937) using ionisation chambers. Later on, with the development of space coronagraphs and neutron monitors, it was shown that CMEs may be the cause of Forbush decreases in the interplanetary medium (Simpson, 1954). Forbush (1954) showed that the variation of the cosmic-ray intensity inversely correlates with the 11-year variation of the solar activity, and with a time lag of few months. Forbush decreases depend on the different phases of the solar cycles and aren't noticed simultaneously at all stations on Earth (Lingri et al., 2016). Observations using neutron monitor detectors are more intense in the geomagnetic poles, independent of atmospheric variability (Arunbabu et al., 2015; Cane 2000), and have exhibited maxima depressions of cosmic ray intensity by 25% (Lingri et al., 2016; Cane, 2000). Moreover, the magnitude of Forbush decrease also depends on solar wind parameters, including, e.g., velocity and magnetic field intensity (Arunbabu et al., 2015).

Usually, Forbush decreases occur in two steps (Ifedili, 2004; Cane, 2000), where a sheath upstream of the CME is led by a fast forward shock. The first step starts at the shock, and the second step occurs with the arrival of the magnetic

cloud. The arrival of the interplanetary disturbance at Earth as a pre-increase of CR intensity caused by the acceleration of high energy charged particles on the outer boundary of an ICME and a pre-decrease due to magnetic connection between the Earth and the region of FD inside of ICME (Belov, 2008). On the other side, less energetic emission cannot create a shock, and it causes one-step Forbush decrease as passes by such small events are too to be recorded by a single neutron monitor. When the propagation of an interplanetary disturbance is faster, and the magnetic field is higher, the Forbush decrease is faster (Belov, 2008). The majority of FDs are sporadic and caused by ICMEs. In this case, decrease in CRI is created by the extension of a disturbed solar wind region that is partly screened from outside by strong and/or transverse magnetic fields (Belov et al., 1997; Belov et al. 1999). Finally, when an ICME travels beyond the Earth orbit, we see the recovery phase of Forbush effect (FE), showing that an expanded disturbed region continues to modulate CRs (Belov, 2008). In other words, as the shock propagates away from Earth, its influence on CR modulation at 1 AU weakens with heliocentric distance, allowing the cosmic ray intensity to gradually recover (Le Roux and Potgieter, 1991).

Forbush decreases can be classified into 3 types: those caused by a shock and ejecta, the one caused by only a shock, and those caused by only ejecta. Maximum decreases (>80%) are given by the two-step type (Cane, 2000). Various researchers have depicted two types of Forbush decreases as non-recurrent decreases and recurrent decreases (Lockwood, 1971; Cane, 2000). Recurrent Forbush decreases have a moderate onset, a symmetric profile, and are associated with CIRs. On the other side, non-recurrent Forbush decreases are usually caused by CMEs, showing a sudden beginning and reaching a maximum depression within a day, with gradual recovery. These have asymmetric profiles and are associated with transient solar wind disturbances (Lingri et al., 2016; Cane, 2000). Occasionally, a Forbush decrease develops with a pre-decrease of about 1 to 3 %, which is observed 3 to 18 hours previous the arrival of the main shock. At this stage, flux usually increases by about 1 to 2%, indicating an incoming decrease, which prevails under the solar wind influence.

Forbush decreases are found to correlate with geomagnetic storms (Lingri et al., 2016), but the clear correspondence and the driver-response relationship is still unclear. For instance, Kane (2010) showed that the magnitudes of geomagnetic disturbances and Forbush decreases are not proportional to each other. Besides, the strong coupling between geomagnetic storms and the solar wind and IMF variability needs to be accounted, so that the complete understanding with Forbush decrease and other parameters, as for example proton velocity, could reveal additional relationships.

In this paper, we have analysed Forbush decreases (FDs) in the CR flux. Moreover, we used the Continuous Wavelet transform (CWT) to find variability and periodicity associated to relative count rate changes of cosmic ray intensity (1-min interval data) during the selected storms. Therefore, the purpose of this work is to validate the wavelet technique as a way to pinpoint the time –

frequency representation and time intervals of these particular spectral components in the FD regions during geomagnetic disturbances. In the next section, we first describe the data and techniques used for the analysis. Then, we show and discuss the results, and finally provide a summary and some suggestions for future works.

2. Data and methods

In this work, we employ space weather data measured during 3 intense geomagnetic storms of the solar cycle 24. Three events were selected based on the responses to the disturbance storm time D_{st} index, which is derived from a network of near-equatorial geomagnetic observatories. The D_{st} index measures the intensity of the globally symmetrical equatorial electrojet, namely the ring current. During geomagnetic storms the ring current intensifies causing a large reduction of the geomagnetic field. In this scheme, minor storms range from -30 nT $> D_{st} > -50$ nT, moderate storms from -50 nT $> D_{st} > -100$ nT, intense storms from -100 nT $> D_{st} > -250$ nT, and great storms from $D_{st} < -250$ nT. The selected storms for this study and corresponding peak values of D_{st} index are listed in Table 1.

Table 1. List of selected storm events along with maximum D_{st} values

Storm	**D_{st} (nT)**
March 17, 2015	-223
June 22, 2015	-208
September 8, 2017	-148

The cosmic ray flux data is obtained from 8 neutron monitor stations distributed over Canada, Russia, Finland, and Greenland. The list of the neutron monitor stations used in this study is shown in Table 1, and the locations can be identified in Figure 1. We use the relative scale of cosmic ray to eliminate the altitude and latitude dependencies. This ensures the consistency of the data despite physical location of neutron monitor stations. The Forbush decreases from each station during the storms are compared to values given during quiet conditions and analysed with the space weather and geomagnetic indices. The space weather and geomagnetic indices include the z-component of interplanetary magnetic field (IMF-B_z), the solar wind speed (V_{sw}), the proton density (N_{sw}), and the D_{st} index.

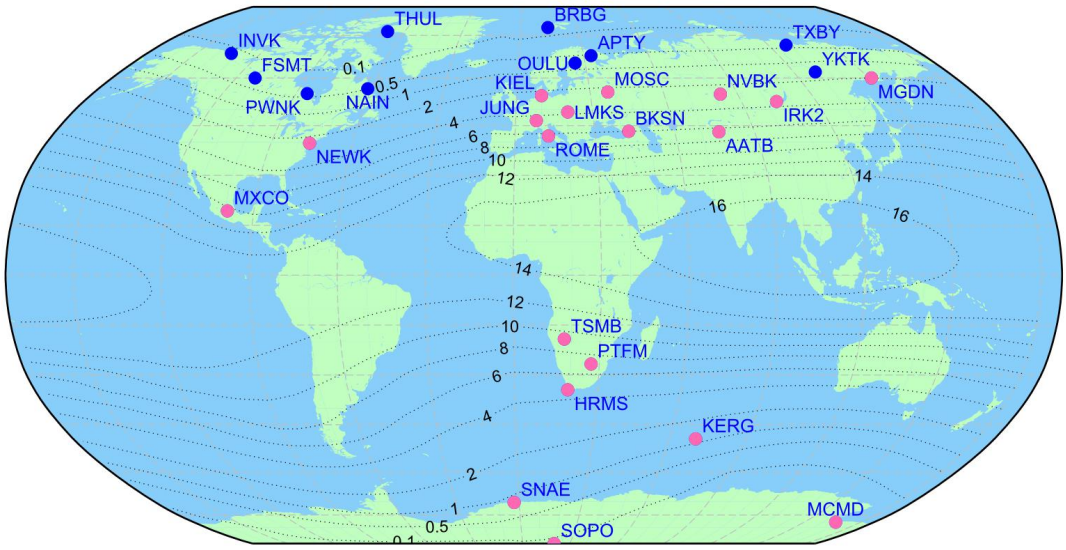

Figure 1 Distribution of the global neutron monitor stations along with the contours of vertical cut-off rigidity at epoch 2000. The contours are in gigavolts (GV). Courtesy of Zhao and Zhang (2016).

Table 2 List of the Neutron Monitor stations used in this study.

Neutron Monitor station	Abbrev.	Location	Longitude (°)	Latitu
Inuvik	INVK	Northwest Territories,Canada	133.72 W	68.36
Fort Smith	FSMT	Northwest territories (NWT), Canada	111.93 E	60.02
NAIN	NAIN	Newfound land And Labrador, Canada	61.68 W	56.55
Irkutsk	IRKT	Irkutsk, Oblast Russia	104.03 E	52.47
Tixie Bay	TXBY	Tixie Bay, Yakutia, Russia	128.54 E	71.36
Yakutsk	YKTK	Yakutsk, Russia	129.43 E	62.01
Oulu	OULU	Oulu, Finland	25.47 E	65.05
Thule	THULE	Thule, Greenland	68.8 W	76.60

In the study, we calculate the Pearson's correlation coefficients and best lineal fit between geomagnetic indices (D_{st} Index and Solar wind velocity) and the cosmic ray flux.

Generally, we encounter two signals; stationary and non-stationary. The stationary signal's frequency content does not change over time, while the frequency of non-stationary changes over time. Majority of raw signals are expressed in their time domain, and the graph representing them is simply a time amplitude representation of that signal. The analysis of signals is used to acknowledge any physical mechanism, and any signal involving access information about the signal's frequency content and the time at which that frequency occurs. Sev-

eral mathematical transformations have been evolved as tools to process these signals and acquire information about them. Fourier transformation (FT) is one of them which deal with the frequency content of signals (Gao and Yan, 2011; Strang, 1993). FT doesn't provide the details on the appearance of these frequencies; understanding the spectral component. Fourier transformation is not preferred for studying the characteristics of non-stationary signals. Wavelet analysis has been rising as an inclusive method to inspect the non-stationary signals and transform the data, operators, or functions into distinct frequency or scale components (Strang and Nguyen, 1996; Foufoula-Georgiou and Kumar, 1995; Daubechies, 1992; Chui, 1992a, b, Mendes et al., 2005). This technique can work with the dynamic window; a window will be narrowed automatically to observe the high-frequency content and be widened to capture the high-frequency content in the signals (Strang and Nguyen, 1996; Foufoula-Georgiou and Kumar, 1995).

During the analysis, the mother wavelet is decomposed into series of basic functions containing dilated and translated mother wavelet functions. Moreover, we use the wavelet transform to study the nonstationary power cosmic ray flux at various frequencies (Daubechies, 1992). CWT is used for non-stationary signals and those signals where it is essential to know which frequency occurred at what instant in time. Many natural signals, including the signals under our consideration fit that category. For a given time-series f(t), wavelet transform is obtained as

$$\mathrm{W}_f^{\psi}(a,b) = \int f(t)\psi_{a,b}(t)^{*}\mathrm{dt} \quad (1)$$

Where $\psi_{a,b}(t)^{*}$ represents the complex conjugate of the wavelet function given by

$$_{a,b}\ (t) = \frac{1}{\sqrt{a}}\psi\left(\frac{t-b}{a}\right) \quad (2)$$

In the above relations, a and b represent the scale and time localization of the wavelet function. This definition of the CWT shows that the wavelet analysis is a measure of similarity between the basic functions (wavelets) and the signal itself. Here the similarity is in the sense of similar frequency content. The calculated CWT coefficients refer to the closeness of the signal to the wavelet at the current scale.

In CWT, low frequencies (high scales) correspond to a global information of a signal (that usually spans the entire signal), whereas high frequencies (low scales) correspond to a detailed information of a hidden pattern in the signal (that usually lasts a relatively short time). Fortunately in practical applications, low scales (high frequencies) do not last for the entire duration of the signal, but they usually appear from time to time as short bursts, or spikes. High scales (low frequencies) usually last for the entire duration of the signal. The wavelet functions are generated by the expansion, (t) $\rightarrow$ (2t), and translation, (t) $\rightarrow$ (t + 1), of simple generator function, (t), called mother-wavelet functions (Meyer, 1990; Souza et al., 2016). For our study, the Morlet wavelet is used

as the generator function, since it has better frequency localization directly comparable with the frequencies observed in Fourier spectrum (Domingues et al., 2005).

The scale, in the above relation either dilates or compresses the signal. If the scale is large, the signal is dilated, while the smaller scales are used for compressed signals. The wavelet is mathematically represented as

$\psi(t) = exp\ \ (\mathrm{i\ t}) \exp\left(\frac{-t^2}{2}\right)$ (3)

Where is the dimensionless frequency (Torrence and Compo, 1998). In order to identify the most energetic periodicities within the time series, the averaged wavelet spectrum is obtained from the local wavelet spectra over the duration of each event (Torrence and Compo, 1998). It is mathematically represented as:

$GWS = \ \frac{1}{N} \sum_{N=0}^{N-1} \left|W_f^{\psi}(a,b)\right|^2$N=0 in uppercase

Where N is the length of the time series.

1. **Results and Discussion**

The storm of 17 March 2015 started few days before the equinox date. This storm was originated from a partial halo CME caused by a magnetic filament explosion at the sunspot no AR2297 (Nayak et al., 2016). This geomagnetic storm is considered the strongest geomagnetic storm of the solar cycle 24. Due to its magnitude, this storm is named St. Patrick's Day geomagnetic storm (Ramsingh et al, 2015).

The storm discerned approximately at 05:00 h UT on 17 March followed by double halo CME (Ramsingh et al.,2015). The occurrence of the CME can be identified by the rapid increase in flow speed and IMF B_z. The solar wind speed increased progressively from approximately 300 km/s (00:00 h UT March 16^{th}) to 430 km/s (05:00 h UT March 17^{th}). Then, at UT=06:00 h, a sudden increase from 430 km/s to 500 km/s shows the arrival of interplanetary shock at the magnetosphere (Liu et al., 2016). After a couple of hours, the solar wind reaches 600 km/s and remains constant until 18 March, when it increases again. At the beginning of the storm, the IMF B_z inclined towards north for a while, indicating the Storm Sudden Commencement (SSC) from UT = 05:00 h-06:00 h. The IMF B_z steadily went back towards north at 12:00 h UT and then turned southward about 12 hours with a magnitude of -20 nT. On 18 March 2015, the IMF B_z turned northward at 00:00 h UT. The D_{st} index raised to +56 nT on 17th March at 06:00 h UT, and then a minimum value of -223 nT was observed on 17^{th} March at 22:00 h UT, same results were also discussed by Fagundes et al. 2016. We can identify 3 phases: (1) initial, (2) main, and (3) recovery phases. The initial phase starts with the SSC on March 17, 2015. Then, from 06:00 to 22:00 h UT on 17^{th} March we identify the main phase. From 22:00 h UT on 17^{th} March recovery phase starts, it has found to be prolonged till 25^{th} March (Jin et al., 2017).

In the bottom panels, we show the hourly-average readings of the neutron monitor stations for the three storms here analysed. The readings are separated in 3 panels, depending on the region they cover. Here, we also include the readings under quiet conditions for comparison (quiets' day on the same month). During this storm, the CME produced a Forbush decrease. In the event, cosmic ray intensity starts decreasing at the early morning and reaches the maximum on 17^{th} March in all eight stations (-2.7 % - INVK, -2.55% - FSMT, -3.1% - NAIN, -2.12% - IRKT, -3.24 % - TXBY, -2.88%- YKTK, -2.98 % - OULU, -2.64 % - THULE). It exhibits the recovery phase after the maximum decrement till the next day. Furthermore, it is known that during an FD, a decrease in CR intensity with amplitude inversely proportional to the cutoff rigidity related to the location of the CR stations observed (Samara et al., 2018).

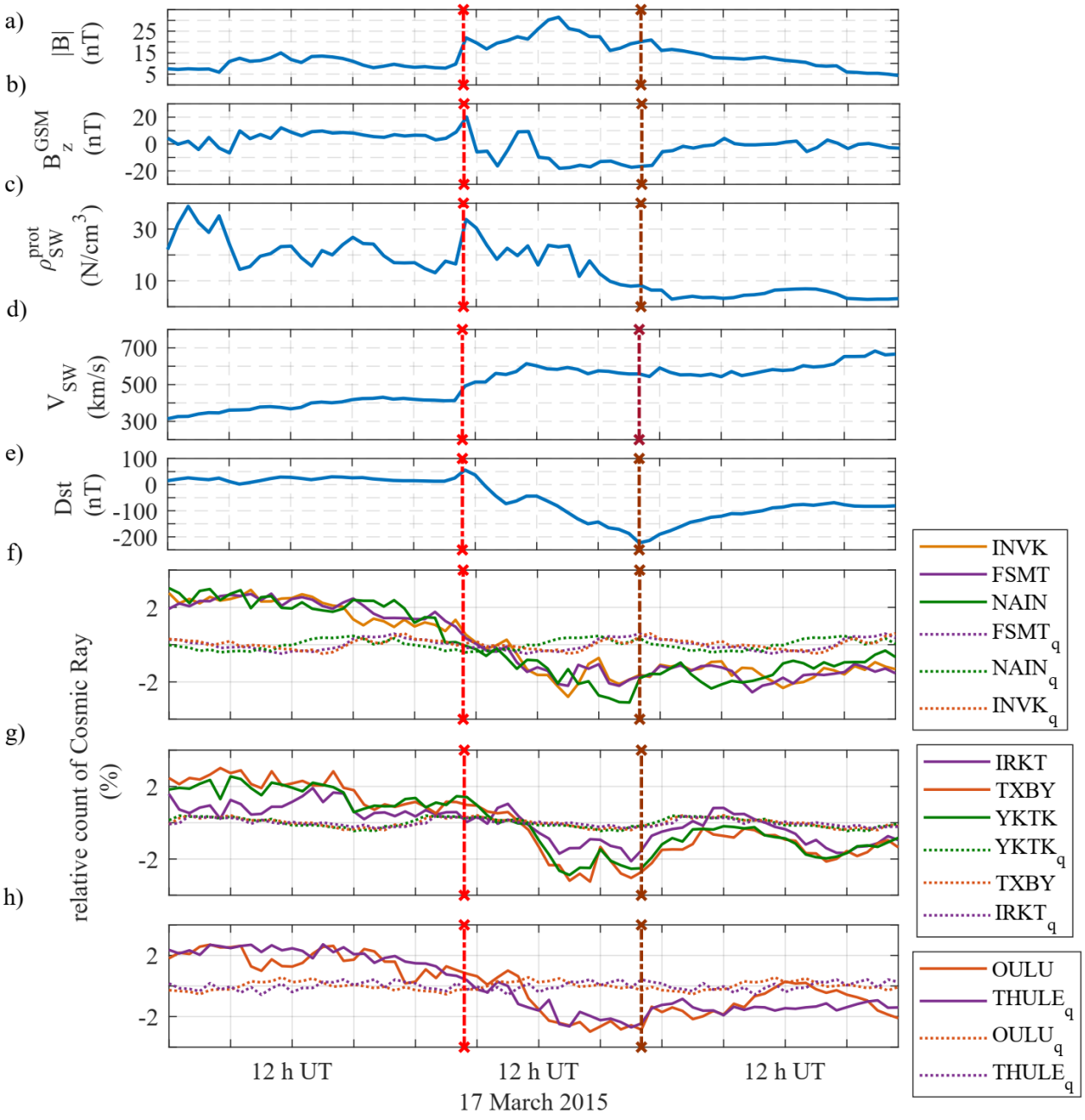

Figure 2 Space weather and geomagnetic indices during the storm of 17 March 2015. From top to bottom, (a) IMB B, (b) IMF B_z (GSM), (c) proton density in solar wind, (d) solar wind velocity, (e) D_{st} index, and (f-h) hourly-average

relative count of cosmic ray for each station. In (f-h), the subscript "q" indicates values during quiet conditions. Vertical dashed lines indicate the time of CME (red color) and the time D_{st} peak (brown color).

The storm of 22 June 2015 had a more complex evolution. Three shocks of different intensities originated in the Sun's active region 2371 were associated with CMEs (Liu et al., 2015). The initial arrival of two shock were observed at 16:50 UT on 21^{th} June and 05:49 UT on 22^{th} June. These shocks were followed by a halo and a partial-halo CME. The third shock is larger than the previous ones, and its arrival is observed at 18:56 UT on 22^{th} June. This shock was associated with a very large full halo CME (Astafyeva et al., 2017). After the entrance of the shock and CME, there was an abrupt loss of energetic particles due to increment in solar wind dynamic pressure (Baker et al., 2016).

Figure 3 shows the sudden change in the solar wind speed, proton density, and an IMF during all 3 shocks. Clear geomagnetic disturbances are seen in the D_{st} index. These were clearly created in response to the southward-directed IMF B_z component, which generated magnetic reconnection and entrance of energy in the magnetosphere-ionosphere system. In the first shock, the solar wind increases to 322 km/s, and the proton density sharply changes from 15 N/cm^3 to 40 N/cm^3. The D_{st} index increased at this SSC to 43 nT. The occurrence of second shock is indicated with an increment in the solar wind speed to 427 km/s, and a change in D_{st} index from 10 nT to 38 nT. Here, the IMF B_z swapped to South direction at -9.77 nT. Then, the appearance of the third shock was accompanied by a giant CME at 18:56 UT on 22^{th} June. A large accretion in the solar wind speed reached 712 km/s, and proton density raised to 40 N/cm^3. The D_{st} index reached a minimum of -207 nT at 4:30 UT on 23 June 2015. The IMF B_z changed its direction several times. Firstly, it was directed southward at the initial phase of the storm from 18:38 to 20:00 UT; then, it reached a minimum of -37.6 nT at 19:20 UT; later, it turned northward during 1.5 h and reached +26.3 nT at 20:30 UT; then, it went to negative from 20:55 UT to 21:15 UT; later, from 21:20 UT it changed to positive until 00:50 UT of the next day, etc. The final large southward event occurred between 08:00 UT to 11:30 UT, and the recovery phase started after 04:30 UT.

The neutron monitor stations recorded a Forbush decrease on 23 June 2015 (Kravtsova et al., 2017). Then, a very short recovery phase began. Forbush decreases and the incoming CMEs connection can be observed in the last three bottom panels of Figure 3. In the event, cosmic ray intensity starts decreases abruptly after the third shock and reaches the minimum on 23^{th} June in all eight stations (-5.47 % - INVK, -5.46% - FSMT, -5.62% - NAIN, -5.16% - IRKT, -4.59 % - TXBY, -5.59%- YKTK, -5.33 % - OULU, -6.41 % - THULE).

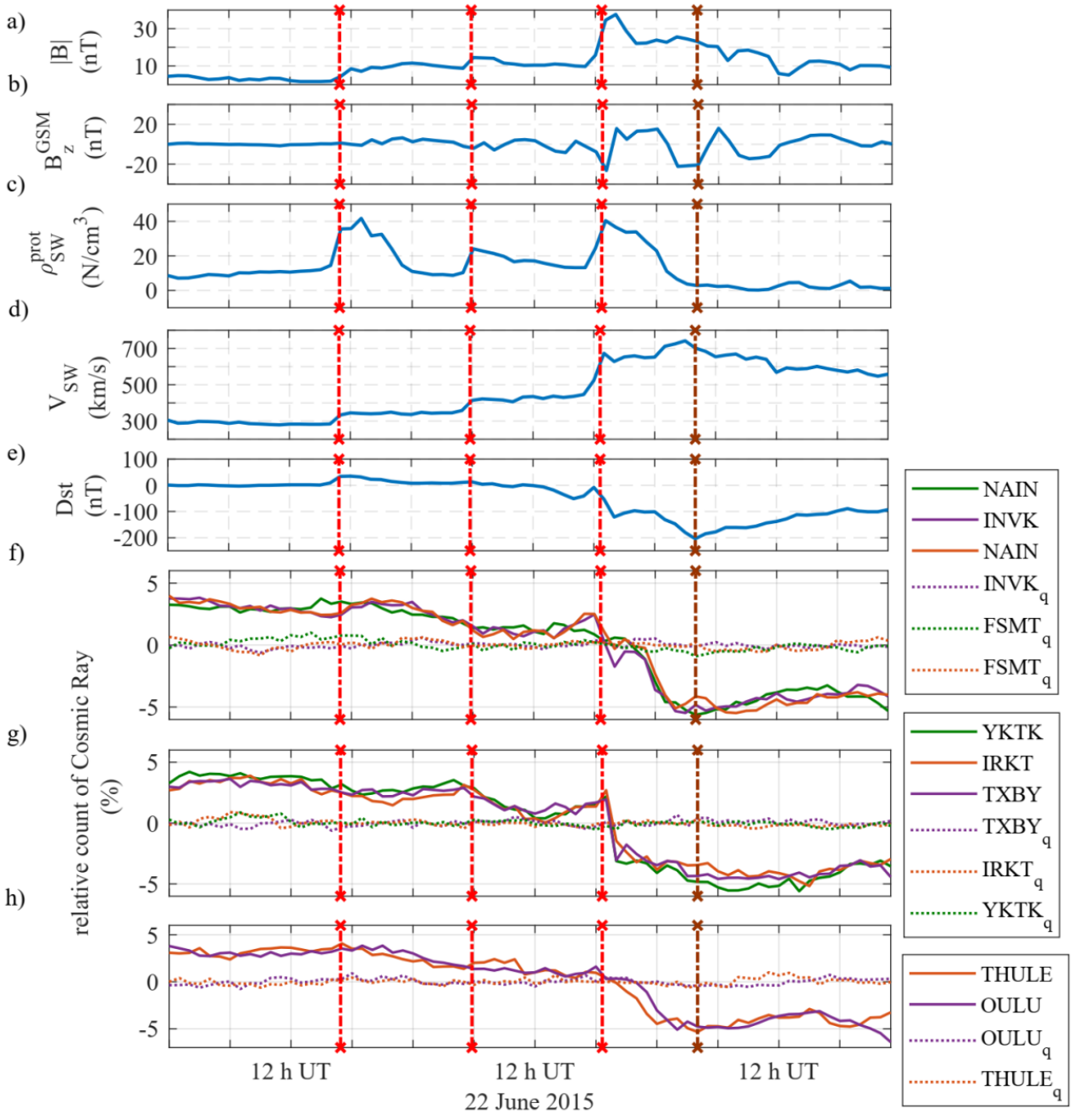

Figure 3 Space weather and geomagnetic indices during the storm of 22 June 2015. From top to bottom, (a) IMB B, (b) IMF B_z (GSM), (c) proton density

in solar wind, (d) solar wind velocity, (e) D_{st} index, and (f-h) hourly-average relative count of cosmic ray for each station. In (f-h), the subscript "q" indicates values during quiet conditions. Vertical dashed lines indicate the time of CME (red color) and the time D_{st} peak (brown color).

On September 4, 2017, a strong activity started in the solar corona with multiple M-flares, from which the strongest reached M5.5. Then, a further X2.2 flare on 6^{th} September was followed by an X9.3 flare. The X9.3 flare was associated with strong radio bursts over a wide range of the frequency spectrum. The CME shock associated to the M5.5 flare on 4^{th} September produced SSC at Earth on 6^{th} September (Mosna et al., 2020).

Among all the M flares recorded, the strongest was M7.3 at 10:15 UT on 7^{th} September. A further X1.3 class flare was observed on 7^{th} September at 14:36 UT (Mosna et al., 2020). Figure 4 shows the events during 7^{th}-9^{th} September, when multiple M-class flares occurred. At this time, the Ionosphere was already under strong influence of the ongoing strong storm that started on 7^{th} September, and the main phase started early on 8^{th} September. Then, Earth was directly influenced by another X8.2 flare at UT= 16:00 on 10^{th} September, showing a decay of X- ray flux until the end of the day. The maximum speed of the solar wind was approximately 820 km/s. The first geomagnetic disturbance started with a SSC at 11:00 UT on 7^{th} September. The main phase of the storm started at 23:00 UT, and the maximum phase occurred at 01:08 UT on 8^{th} September. Then, the storm reached its maximum disturbance at around 13:56 UT on 8^{th} September. This CME reached the Earth relatively soon, indicating that the IMF was already preconditioned by previous CMEs. The first decrease in the D_{st} index indicates the onset of the storm, and its associated ejecta arriving at 23:00 UTC with a southward IMF B_z of approximately 10 nT. Then, the IMF B_z pointed to South with a value of 30 nT, and D_{st} sharply decreased to a minimum of approximately -150 nT.

As a result of this storm, a deep Forbush decreases in the galactic cosmic ray flux was recorded by the neutron monitor stations. In the maximum phase, the Forbush decrease reaches approximately -5 to -6 % at most of the selected stations in Figure 4. Cosmic ray intensity drops abruptly after the second CME and reaches the minimum on 8^{th} September in all eight stations (-5.28 % - INVK, -5 % - FSMT, -4.33% - NAIN, -5.21% - IRKT, -5.10 % - TXBY, -6.19%- YKTK, -5.31 % - OULU, -4.53 % - THULE). In Figure 4, Forbush decreases are clearly distinguishable, where the second one shows a classical two-step evolution (Hubert et al., 2019) on 9^{th} September. Second Forbush decrease seen exhibited -2 to -3% decreases in all eight stations.

From Figures 2-4, we can observe that all the neutron monitor stations exhibited a clear decreasing after the occurrence of the CMEs. For all cases, the Forbush decrease is clearly correlated with the D_{st} and solar wind variation, showing some time-lag. The decrease usually starts with the arrival of the shock at the magnetopause, and then the Earth enters a period of reduced particle influx. Therefore, comparing with the data of quiet days, all cases show a pre-increase

in cosmic ray of about 2-3%, which can be associated to the onset of the storm. The pre-increases are usually of very short duration (i.e., few hours), although it may also extend to longer periods. Then, a recovery phase from the Forbush decrease occurs after the main shock.

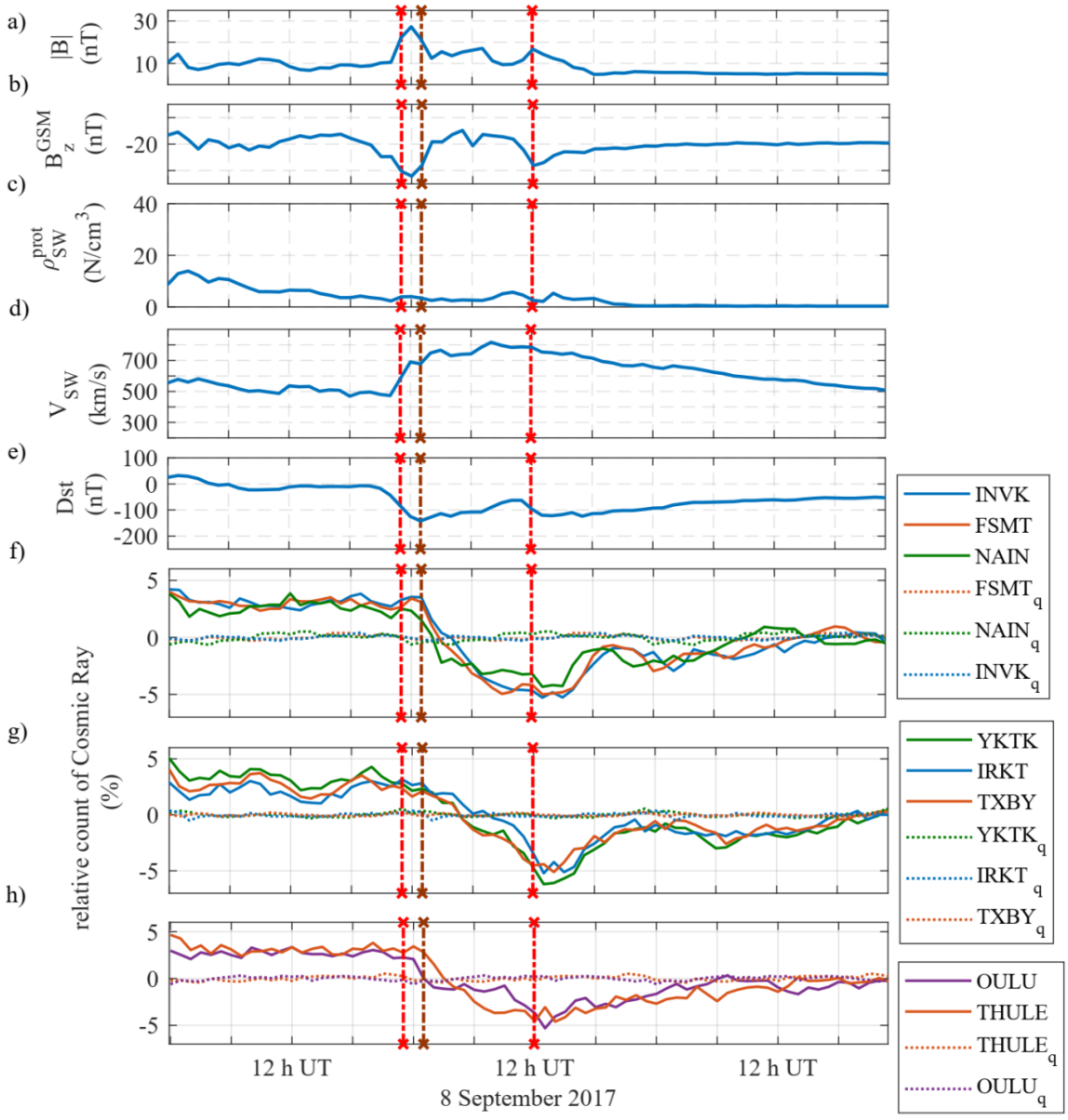

Figure 4 Space weather and geomagnetic indices during the storm of September 8, 2017. From top to bottom, (a) IMB B, (b) IMF B_z (GSM), (c) proton density

in solar wind, (d) solar wind velocity, (e) D_{st} index, and (f-h) hourly-average relative count of cosmic ray for each station. In (f-h), the subscript "q" indicates values during quiet conditions. Vertical dashed lines indicate the time of CME (red colour) and the time D_{st} peak (brown colour).

In this paper, we analysed a Forbush decrease in a time-scale plane. In wavelet analysis, we call it wavelet scalogram exhibiting time-frequency representation. Figures 5 to 7 depict the spectral features of the Forbush decreases during the storms at the selected neutron monitor stations, the horizontal axis represents the time in hours and the vertical axis represents the periodicity in minutes. The square modulus of the wavelet coefficient provides the energy distribution in the time-scale plane, which is analogous to Fourier analysis.

The amplitudes depicted in the plot, whose colours are demonstrated on the bottom part of the figures, represent the squared estimation of relative count rate changes of cosmic ray intensity data. In the scalogram, areas of stronger wavelet power are shown in red (horizontally on the bottom) and the areas of low wavelet power are shown in blue. Scrutinizing the scalograms, the characteristic relative count rate changes of cosmic ray intensity demonstrates high variability with time without presence of continuous periodicities. The power ranges of higher intensity are seen at various time scales on selected events.

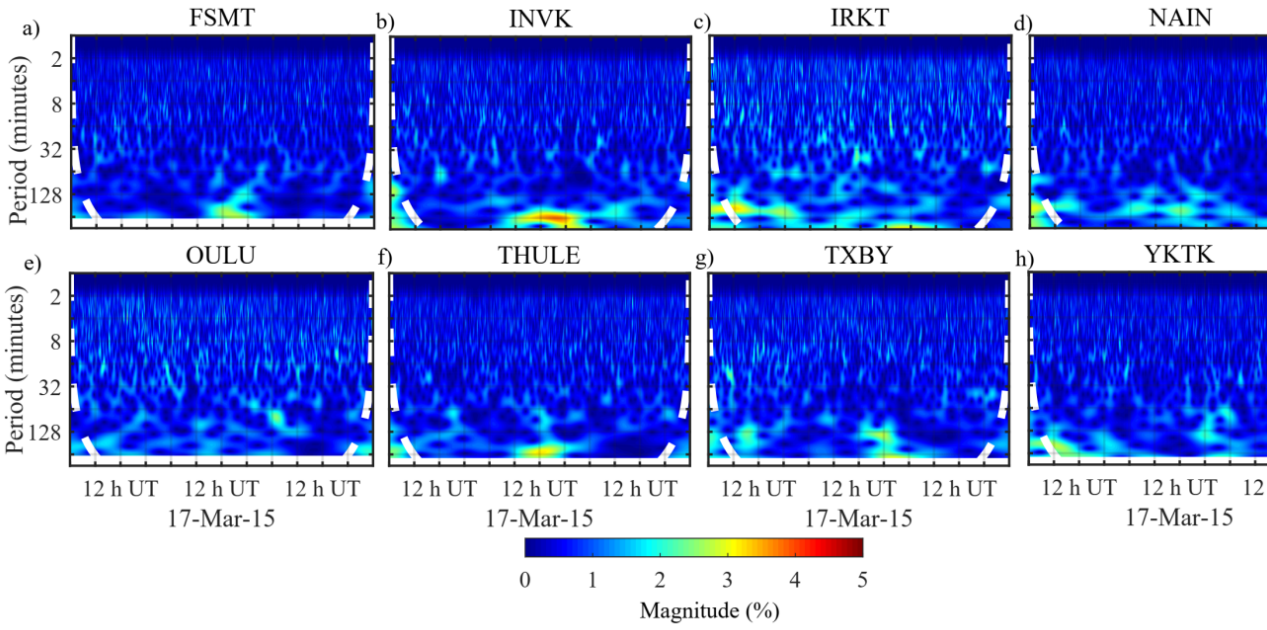

Figure 5 Wavelet scalogram of relative count rate changes of cosmic ray intensity (1-min interval data) during the storm of March 17, 2015.

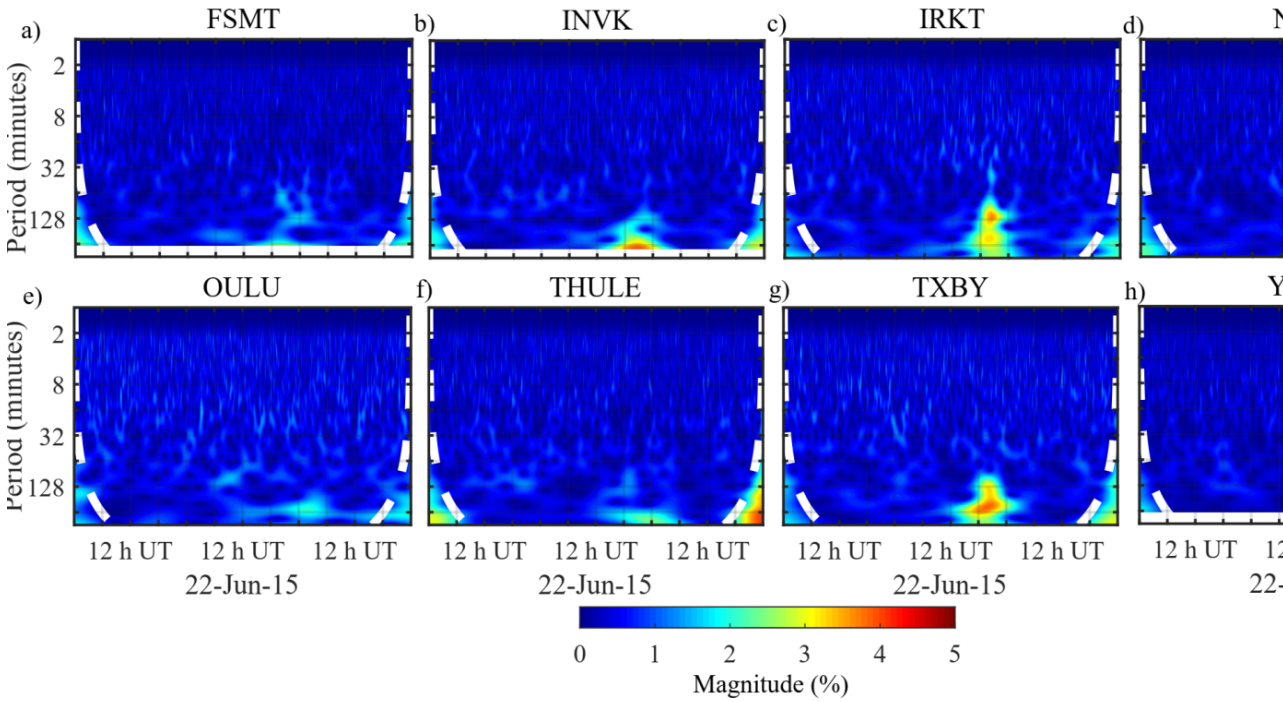

5 represents the result of scalogram of relative count rate changes of cosmic ray intensity (1-min interval data) event on 16-18 March, 2015. In the figure, the horizontal axis represents the time in hours and the vertical axis represents the period in minutes. The scalogram shows a strongest wavelet power area from, approximately 12:00 UT 17th March – 00:00 UT 18th March on Canadian stations (INVK, FSMT, NAIN). The physical phenomena responsible for wavelet power area appears to have a period of 128 minutes approximately. Similarly, strongest wavelet power area at Russian stations (IRKT, TXBY, YKTK), OULU and THULE were seen from 18:00UT 17th March – 08:00 UT 18th March, 00:00 UT – 08:00 UT 18th March and 06:00 UT – 18:00 UT 17th March. Wavelet power areas appear to have periods of approximately 64-256 minutes, 64 minutes and 64 minutes respectively. Wavelet graphs indicate the 2-3 % decrease in the magnitude of cosmic ray flux as supported by the graph plotted in Figure 2.

Figure 6 Wavelet scalogram of relative count rate changes of cosmic ray intensity (1-min interval data) during the storm of 22 June 2015.

Correspondingly, Figures 6 and 7 represent the result of scalogram of relative count rate changes of cosmic ray intensity (1-min interval data) event on 21-23 June, 2015 and 7-9 September 2017. The scalograms of 21-23 June exhibits a strongest wavelet power area from, approximately 13:00 UT 22 June – 06:00 UT 23June on Canadian stations (INVK, FSMT,NAIN), Russian stations (IRKT,

TXBY, YKTK) and THULE evincing periods of approximately 64-256 minutes, 32- 256 minutes and 256 minutes respectively. OULU displays strongest wavelet power area from 19:00 UT 22 June – 06:00 UT 23 June with periodicity of 128 minutes. Most of the scalograms (INVK, IRKT, TXBY and YRKT) indicate about 5% decrease in the magnitude of cosmic ray flux as supported by the graph plotted in Figure 3.

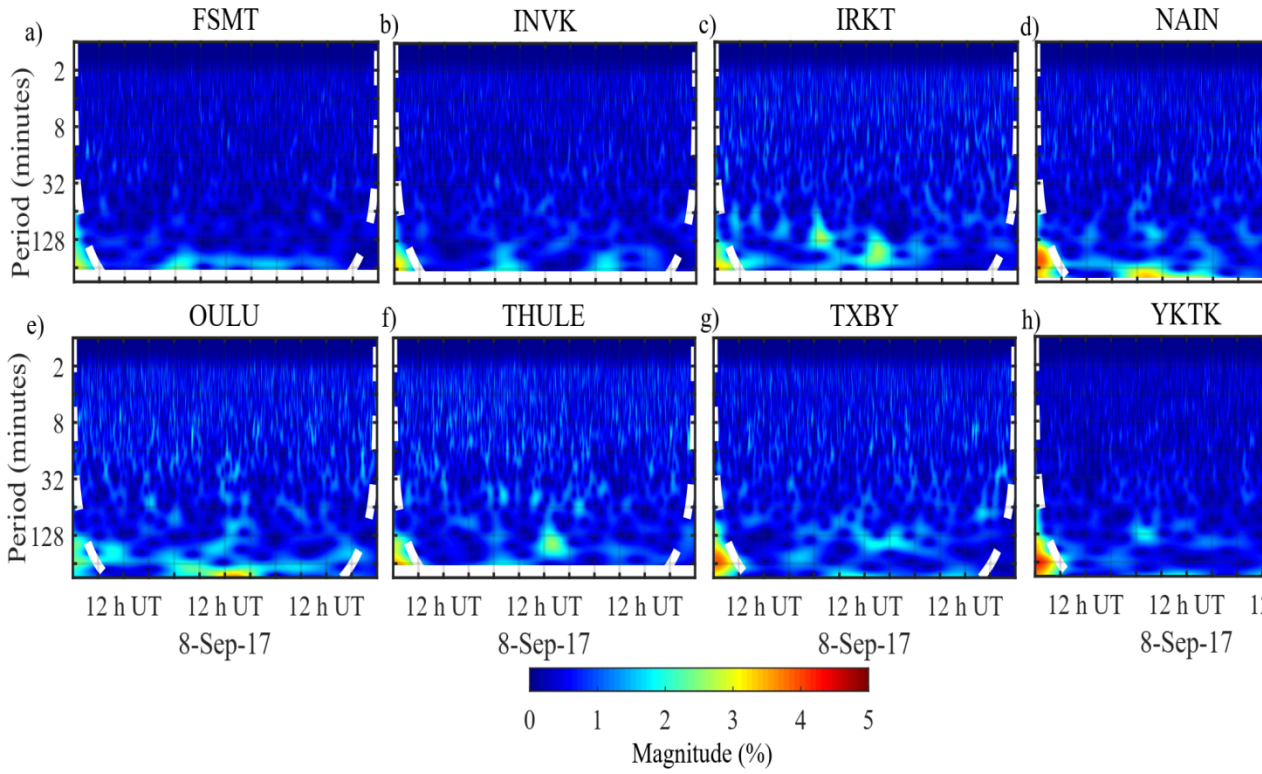

Figure 7 Wavelet scalogram of relative count rate changes of cosmic ray intensity (1-min interval data) during the storm of September 8, 2017.

Figure 7 exhibits uneven wavelet power area in all the selected stations. Scalogram of INVK indicates wavelet power at two distinct areas from 00:00 UT – 06:00 UT on 8th and 9th September, having period of 128 minutes respectively. FSMT exhibits wavelet power area from 0:00 UT 8th September- 00:00 UT 9th September with periodicity of 128 minutes where magnitude of cosmic ray flux is stronger at 0:00 UT - 06:00 UT 8th September. Scalogram of the NAIN displays the wavelet power areas from 19:00 UT 7th September – 18:00 UT 8th September with periodicity of 256 minutes. It also has two positions where the decrement magnitude of cosmic ray flux is high (00:00 UT – 06:00 UT and 12:00 UT – 18:00 UT 8th September). Scalogram of IRKT exhibits wavelet power areas from 00:00 UT – 18:00 UT 8th September and 12:00 UT -18:00 UT

with respective periods of 64 minutes and 128 minutes respectively. Scalogram of TXBY has wavelet power areas from 07:00 UT -13:00 UT 8th September and 13:00 UT 8th September - 00:00 UT 9th September with periodicity of 256 minutes and 128 minutes respectively. Scalogram of YKTK has faint wavelet power areas from 00:00 UT - 05:00 UT 8th September with respective periodicity of 128 minutes. Scalogram of OULU exhibits wavelet power area from 00:00 UT 8th September -12:00 UT 9th September where the strong power area can be seen distinctly 13:00 UT – 18:00 UT 8th September with periodicity of 256 minutes. THULE has strong power areas from 12:00 UT – 18:00 UT 8th September with periodicity of 128 minutes. INVK, IRKT and NAIN has two different distinct positions of strong power areas in order to support the two - step Forbush decrease of the event.

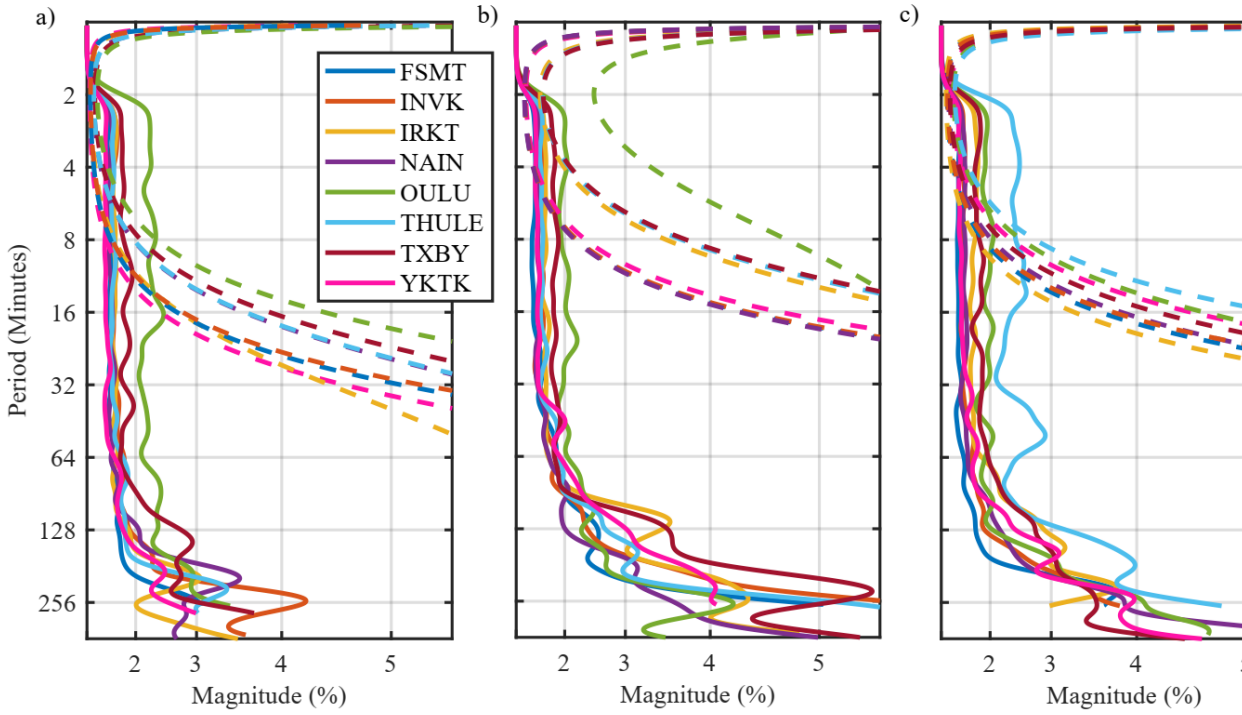

Figure 8 The averaged wavelet spectrum for (a) 17 March 2015, (b) 22 June 2015, and (c) 8 September 2017.

The power areas with lower intensity can also be seen at different times and scales in the scalograms. Figure 5-7 shows the development of decrease in cosmic rays' flux with respective periods. Thus, it may be said that the decrement presented in figures is arising from the geomagnetic disturbances supported by the decrement in D_{st}-Index and increment of V_{sw} at the respective time scale. These results reveal wavelet analysis describes the distribution of energy of whole

signal through time. We found distinct periodicity in decrement of cosmic ray flux associated with the selected geomagnetic storms.

Figure 8 shows the averages of the wavelet spectrum for each case. In general, the main periodicities are around 256 and 128 minutes. We can investigate the central frequencies (or central periods) of the time series called pseudo-frequencies (or pseudo periods) through the global wavelet spectrum. The behaviour of the energy at a certain scale can be understood by GWT (Klausner et al., 2013). We can notice that maximum and minimum wavelet power on the scalogram correspond to high and low pronounce peak on global wavelet spectrum simultaneously.

Figure 9 shows the correlation-delay analyses performed between the relative count rate changes of cosmic ray intensity against the D_{st} index and the solar wind velocity (V_{sw}). Other parameters provided lower correlations and are not included in this analysis. Cross-correlation analysis are useful for analysing the relationship between the D_{st} index and Solar wind velocity with FDs and testing the dataset. We aligned two-time series, one of which is delayed with respect to the other, as its peak occurs at the lag at which the two-time series are best correlated, that is, the lag at which they best line up (Menke and Menke, 2012).

In Figure 9, similar peak correlations are given for all stations in each 6 cases, but the lag/lead times show a large discrepancy for the D_{st} index and V_{sw} for the different storms. The curves attained a maximum cross-correlation coefficient with D_{st} from 0.70 – 0.92 at time lag 2-6 hours during the event 17th March 2015. V_{sw} showed disproportionate association with FD with a correlation coefficient ranging from 0.80 - 0.94 with a lag of 4-6 hours during the event. Similarly, positive correlation coefficient with D_{st} was seen ranging from 0.91 – 0.94 with 0-2 h lag and 0.82 – 0.86 with 3-9 h lag on 22nd June 2015 and 8th September 2017. Negative correlation coefficient with V_{sw} ranging from 0.95-0.97 with 3-6 h lag and 0.80-0.87 with 0-5 h lag was seen on respective events. The positive lag advises that the second signal features (CR intensity) occur at later times than corresponding features in the first signal (D_{st}/V_{sw}). The less value of lag occurs when a sudden decrease in CR intensity responds quicker to the change in D_{st}/V_{sw}. In all the observed cases, as visible in the figure, D_{st}/V_{sw} correlates with the deviation in cosmic ray flux at a relatively more minor lag value, concluding that all the stations exhibit a similar pattern during a particular event of study. It is interesting to notice the high correlation found in all the series. Lag-times for the D_{st} index on September 2017 are approximately -5 hours; on June 2015 are approximately 0 hours; and on March 2015 are approximately +5 hours. On the other side, time-lags for the solar wind velocity show similar values being approximately -4 hours for all cases. Table 3 shows the maxima correlations and corresponding delay-times for each case.

As the CME overwhelms the Earth, we witnessed FD due to the deflecting effects of distorted magnetic fields detected by cosmic ray detectors (Arunbabu et al., 2013). During the process, cosmic ray flux was collated with V_{sw} values and the D_{st} index. It indicates a clear association between the V_{sw} and the

D_{st} index with the FD, leading to the view that FDs and D_{st} depression along with soaring V_{sw} values could be correlated with the same physical mechanism. The different nature of time lag during the events may prevail due to the effects of many nonlinear processes and external forcing, causing the signals to have multi-scale structures and non-stationarities (Barnett, 1991; Huang et al., 1998).

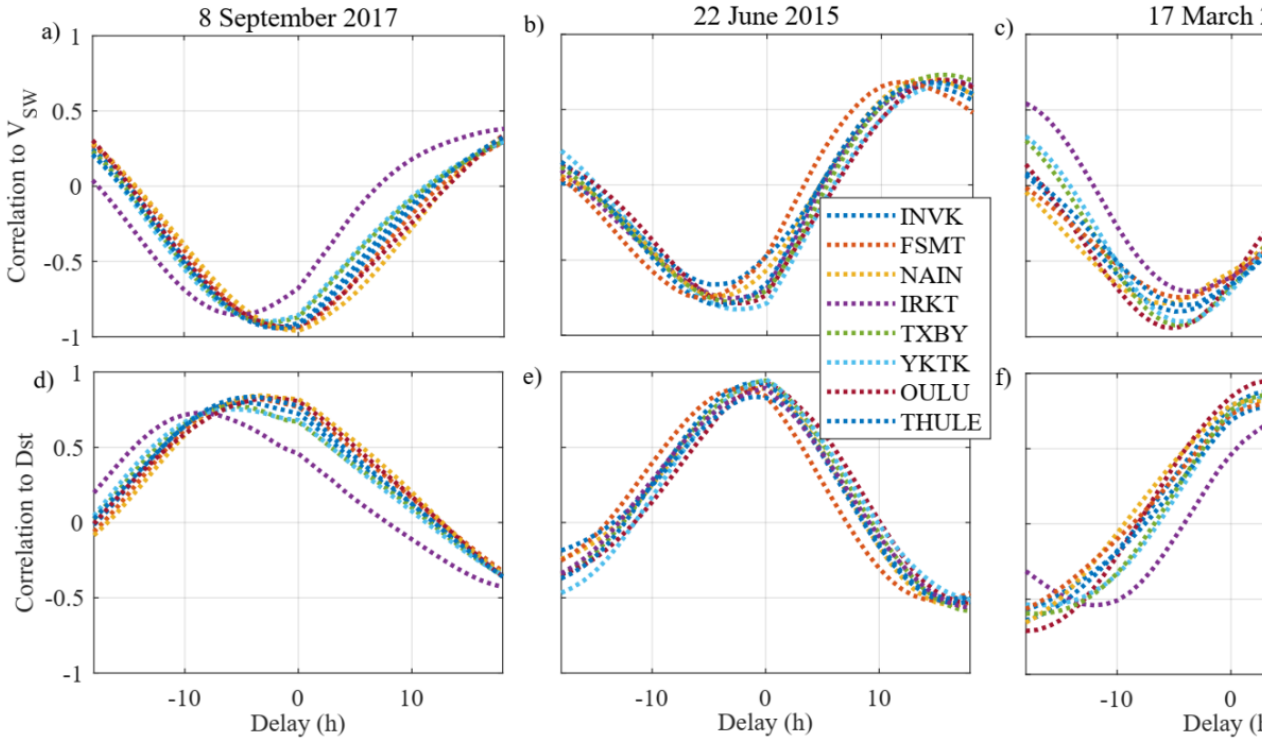

Figure 9 The correlation-delay plots between the relative count rate changes of cosmic ray intensity against (a-c) Solar wind velocity (V_{sw}) and (d-f) D_{st} index for the 8 Monitor stations during the geomagnetic storms of March 2015 (c,f), June 2015 (b,e), and September 2017 (a,d).

Table 3. Delay at maxima correlation between relative count rate changes of cosmic ray intensity and (1) -Dst index and (2) Solar Wind Velocity (V_{sw}) for the 8 selected stations during the 3 geomagnetic storms.

	17-Mar-15		**22-Jun-15**		**8-Sep-17**			
ID	**Dst Corr.**	**Vsw Delay (h)**	**Dst Corr.**	**Vsw Delay (h)**	**Dst Corr.**	**Vsw Delay (h)**	**Corr.**	**Delay (h)**
INVK	0.86	4	0.94	-4	0.93	-1	0.96	-4
FSMT	0.88	3	0.93	-4	0.93	-2	0.97	-6
NAIN	0.9	2	0.91	-6	0.94	0	0.97	-6

	17-Mar-15	**22-Jun-15**	**8-Sep-17**					
IRKT	0.73	6	0.8	-4	0.91	0	0.96	-3
TXBY	0.89	4	0.94	-5	0.94	0	0.96	-4
YKTK	0.89	4	0.92	-4	0.94	0	0.97	-3
OULU	0.91	3	0.9	-5	0.94	0	0.97	-3
THULE	0.92	4	0.93	-5	0.92	-1	0.95	-4

In Figures 10-11, the scatter plots between the relative count rate changes of cosmic ray intensity against D_{st} index (Figure 10) and the solar wind velocity (Figure 11) for the 8 neutron monitor stations are shown for the 3 geomagnetic storms here investigated. For all cases, the clouds of samples show a linear dispersion, which has been parameterized and included in solid lines for better visualization. Table 4 shows the linear-fit parameters for all cases. In Figure 10, clear discrepancies are seen for the storm of March 2015, showing a lower inclination than that given for the storms of September 2017 and June 2015. On the other side, in Figure 11, the parameterization in terms of solar wind velocity show much more similar inclinations, but with different biases. These biases suggest the need of an additional dependence that might modulate the strength of the Forbush decrease. For instance, for similar values of solar wind, note the stronger Forbush decreases for the storms of June and March 2015, when comparing with that seen during the storm of September 2017. Figures 2-4 suggest that a possible parameter candidate could be the proton density, which shows very low values during the storm of September 2017, in comparison to the other two storms. It is highly probable that high values of proton density in the solar wind may produce lower flux of cosmic ray under similar solar wind velocity, thus creating larger Forbush decreases.

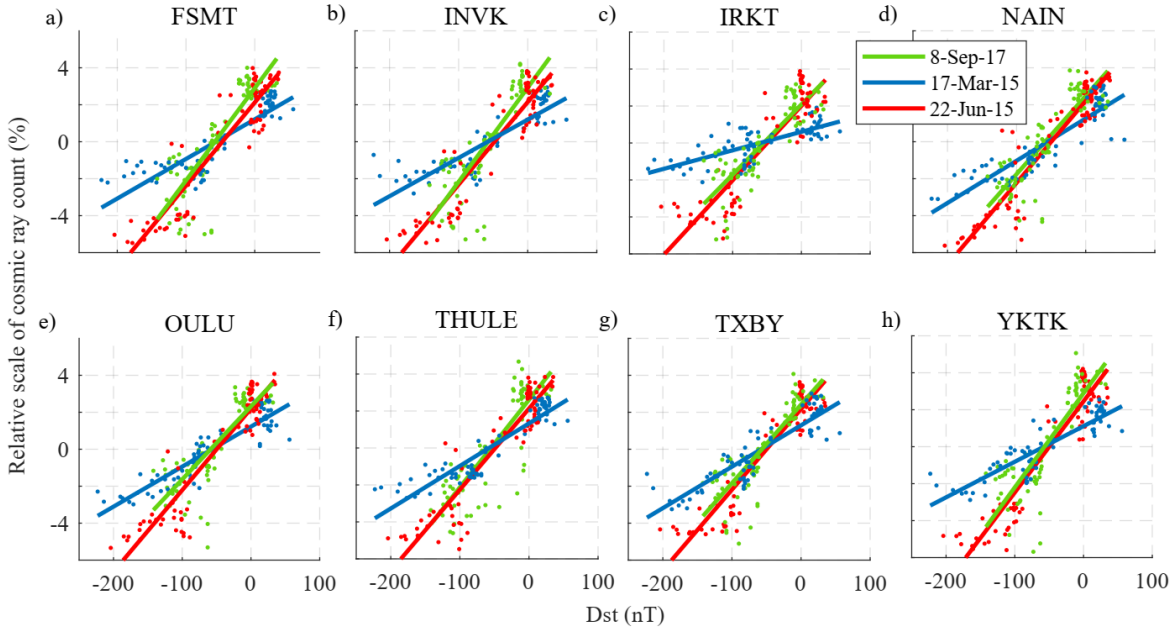

Figure 10 Scatter plot of relative count rate changes of cosmic ray intensity against Dst Index for the 8 neutron monitor stations during the geomagnetic storms of March 2015 (blue), June 2015 (red), and September 2017 (green). The linear fits are included in solid lines, and the corresponding fit-parameters are given in Table 4.

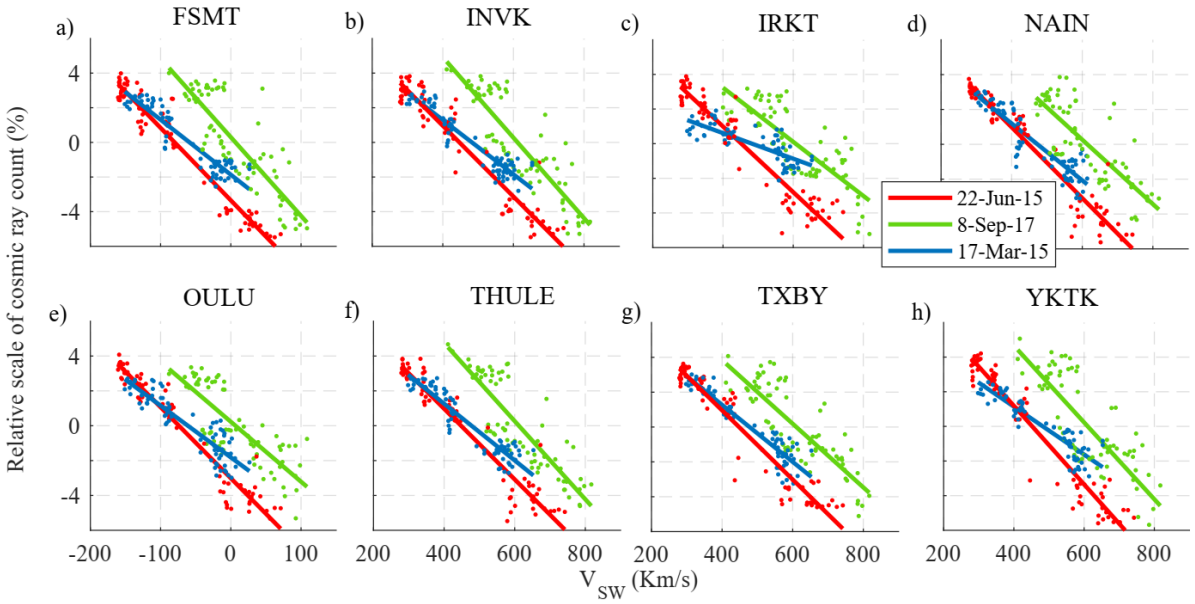

Figure 11 Scatter plot of relative count rate changes of cosmic ray intensity against Solar Wind Velocity (V_{sw}) for the 8 neutron monitor stations during the geomagnetic storms of March 2015 (blue), June 2015 (red), and September 2017 (green). The linear fits are included in solid lines, and the corresponding fit-parameters are given in Table 4.

Table 4. Coefficients and R^2 parameter for the linear fit (a*x+b) between relative count rate changes of cosmic ray intensity and (1) $-D_{st}$ index and (2) Solar Wind Velocity (V_{sw}) for the 8 selected stations during the 3 geomagnetic storms.

		17-Mar-15	**22-Jun-15**	**8-Sep-17**						
ID	**proxy**	**a**	**B**	**R^2**	**A**	**B**	**R^2**	**A**	**b**	**R^2**
INVK	D_{st}	0.0207	1.2	0.74	0.045	2.1	0.87	0.0509	2.9	0.72
	V_{sw}	-0.0157	7.6	0.88	-0.020	9.1	0.92	-0.0232	14.2	0.75
FSMT	D_{st}	0.0214	1.2	0.77	0.045	2.1	0.86	0.0500	2.9	0.71
	V_{sw}	-0.0159	7.7	0.87	-0.021	9.2	0.95	-0.0227	13.9	0.72
NAIN	D_{st}	0.0229	1.3	0.81	0.044	2.2	0.88	0.0423	2.5	0.71
	V_{sw}	-0.0163	7.7	0.82	-0.020	9.1	0.93	-0.0185	11.3	0.65
IRKT	D_{st}	0.0100	0.6	0.54	0.040	2.0	0.82	0.0379	2.1	0.71
	V_{sw}	-0.0074	3.6	0.63	-0.019	8.6	0.92	-0.0156	9.5	0.65
TXBY	D_{st}	0.0224	1.3	0.80	0.044	2.2	0.89	0.0425	2.4	0.73
	V_{sw}	-0.0164	7.8	0.88	-0.020	8.9	0.93	-0.0183	11.1	0.70
YKTK	D_{st}	0.0193	1.1	0.78	0.049	2.5	0.89	0.0510	2.9	0.68
	V_{sw}	-0.0138	6.7	0.84	-0.023	10.3	0.94	-0.0222	13.5	0.67
OULU	D_{st}	0.0217	1.2	0.83	0.044	2.2	0.88	0.0395	2.3	0.68

		17-Mar-15	22-Jun-15	8-Sep-17						
	V_{sw}	-0.0149	7.1	0.80	-0.020	9.2	0.94	-0.0172	10.5	0.64
THULE	D_{st}	0.0230	1.3	0.84	0.044	2.1	0.85	0.0473	2.6	0.71
	V_{sw}	-0.0163	7.8	0.87	-0.020	9.1	0.91	-0.0224	13.7	0.76

1. Summary and Conclusions

There is a close relation between solar activity and cosmic ray flux recorded by the ground-based neutron monitor stations (Shrivastava et al., 2005). This work has investigated the spectral features of Forbush Decrease during intense geomagnetic storms as seen from 8 stations globally distributed. More in detail, our conclusions are summarized as follows:

- The storm of 15 March 2015 created modulation of the galactic cosmic ray flux resulting in Forbush decreases in approximately 3 to 4 % during more than 3 days. The ramification of strike in the Earth's magnetosphere was perfected at 04:45 UT from a partial halo CME derived from magnetic filament explosion at the sunspot no AR2297 (Gosling et al., 1991). During the storm of 23 June 2015 three interplanetary shocks with different intensities and originated in the Sun's active region 2371 are associated with CMEs. During this storm, a small Forbush decrease was recorded from ground stations. The D_{st} peak reached -207 nT at 4:30 UT. During the storm of 6-8 September 2017, the X2.2 and X.9.3 flares were associated with CMEs and prorogued a decrease of the D_{st} index down to –150 nT. As a result of the two flares, a deep Forbush decrease was recorded in the galactic cosmic ray flux, showing a 6% decrease over all the selected stations.
- The spectral analysis of Forbush decreases during the storms at the 8 selected stations showed similar periodicities (~2 hours) for the classical two-step process in the Forbush decrease. Slightly distinct decreases were shown by the IRKT and INVK stations. Note the IRKT station exhibited low correlation for all the events and it could be excluded from the analysis. Correlation-delay analyses with space weather and geomagnetic indices have shown that V_{sw} and D_{st} index have significant correlation with cosmic ray flux, with values above 0.9 for the storms of March and June 2015, and about 0.85 for the storm of 8 September 2017. We obtain similar time-delay responses to the solar wind velocity for all the cases (~4 hours), but large discrepancies are seen for the D_{st} index between the storms. We therefore recommend not using the D_{st} index for predicting Forbush decreases.
- We parameterize the Forbush decreases in terms of solar wind and D_{st}, and we obtain a predictive model with R^2 parameter of approximately 0.8. We observe a possible dependence on solar wind proton density, which modulates the magnitude of Forbush decreases under similar solar wind velocity conditions.

Our results verify the suitability of using solar wind parameters against D_{st} index to predict Forbush decreases in the cosmic ray flux. An important result that came out from the overall analysis was that there exists a wavelet signature that clearly identifies the main phase of a geomagnetic storm period, for intense magnetic storms. The advantage of the time-frequency analysis method called Wavelet Transform resides in providing information not only about the frequencies of the event but also about its location in the time series.

Acknowledgments

Geomagnetic index SYM-H and solar wind parameter IMF-Bz are obtained from the OMNI (https://omniweb.gsfc.nasa.gov/form/dx1.html) site. In addition, cosmic ray intensity data of eight different stations, corrected for pressure and efficiency, are downloaded from NMDB Database (https://www.nmdb.eu/). We acknowledge the NMDB database, founded under the European Union's FP7 programme (contract no. 213007) for providing data. Great appreciation is extended to NEST, NASA, and ISGI for the space weather and geomagnetic indices.

Author Contributions

Rabin Baral and Binod Adhikari presented the idea for the paper. Rabin Baral carried out the methodology, data processing, and draft preparation; Binod Adhikari and Roshan Mishra verified the analytical methods. Andres Calabia provided supervision, mentorship, funding support and computational resources as well as undertook revision tasks; Roshna Manandhar and Sudarshan Bohara carried out manuscript editing and revision tasks. Munawar Shah, Luis del Peral and María D. Rodríguez Frías contributed to the final version of the manuscript.

Competing interests

The authors declare no competing interests.

Data Availability Statement

The space weather data are available from the website of the Low Resolution OMNI (LRO) data set of NASA, http://omniweb.gsfc.nasa.gov/form/dx1.html. The geomagnetic data are available from the International Service of Geomagnetic Indices (ISGI), http://isgi.unistra.fr/data_download.php. The cosmic ray data was acquired from the Neutron monitor data base Event Search Tool (NEST), http://www01.nmdb.eu/nest/. All data supporting the findings of this study will be available upon request.

References

Ahluwalia, H. S. (2003), Solar wind modulation of galactic cosmic rays, *Geophys. Res. Lett.*, 30, 1133, doi:10.1029/2002GL016017, 3.

Arunbabu, K. P., Antia, H. M., Dugad, S. R., Gupta, S. K., Hayashi, Y., Kawakami, S., ... & Subramanian, P. (2015). How are Forbush decreases related

to interplanetary magnetic field enhancements?. Astronomy & Astrophysics, 580, A41.DOI: https://doi.org/10.1051/0004-6361/201425115

Arunbabu, K.P., Antia, H.M., Dugad, S.R., Gupta, S.K., Hayashi, Y., Kawakami, S., Mohanty, P.K., Nonaka, T., Oshima, A. and Subramanian, P.: 2013, High-rigidity Forbush decreases: due to CMEs or shocks? *Astronomy & Astrophys.* **555**, p.A139 DOI:https://doi.org/10.1051/0004-6361/201220830

Astafyeva, E., Zakharenkova, I., Huba, J. D., Doornbos, E., & Van den IJssel, J. (2017). Global ionospheric and thermospheric effects of the June 2015 geomagnetic disturbances: Multi-instrumental observations and modeling. Journal of Geophysical Research: Space Physics, 122(11), 11-716.https://doi.org/10.1002/2017JA024174

Astafyeva, E., Zakharenkova, I.,Hozumi, K., Alken, P., Coïsson, P.,Hairston, M. R., & Coley, W. R. (2018).Study of the equatorial and low-latitudeelectrodynamic and ionosphericdisturbances during the 22–23 June2015 geomagnetic storm usingground-based and spacebornetechniques. Journal of GeophysicalResearch: Space Physics, 123, 2424– 2440.https://doi.org/10.1002/2017JA024981

Baker, D. N., Jaynes, A. N., Kanekal, S. G., Foster, J. C., Erickson, P. J., Fennell, J. F., ... & Wygant, J. R. (2016). Highly relativistic radiation belt electron acceleration, transport, and loss: Large solar storm events of March and June 2015. Journal of Geophysical Research: Space Physics, 121(7), 6647-6660. https://doi.org/10.1002/2016JA022502

Baker, D. N., Jaynes, A. N., Turner, D. L., Nakamura, R., Schmid, D., Mauk, B. H., ... & Burch, J. L. (2016). A telescopic and microscopic examination of acceleration in the June 2015 geomagnetic storm: Magnetospheric Multiscale and Van Allen Probes study of substorm particle injection. Geophysical Research Letters, 43(12), 6051-6059. https://doi.org/10.1002/2016GL069643

Barnett, T. P. (1991). The interaction of multiple time scales in the tropical climate system. Journal of Climate, 4(3), 269-285. DOI: https://doi.org/10.1175/1520-0442(1991)004<0269:TIOMTS>2.0.CO;2

Belov, A. V., Eroshenko, E. A., & Yanke, V. G. 1997, Correlated Phenomena at the Sun, in the Helosphere and in Geospace, 463

Belov, A. V., Eroshenko, E. A., & Yanke, V. G. 1999, Proc. 25th ICRC, 6, 431

Belov, AV: 2008, Forbush effects and their connection with solar, interplanetary and geomagnetic phenomena. Proceedings of the International Astronomical Union. 4(S257), 439–450. doi:10.1017/s1743921309029676

Cane, H. V. (2000). Coronal mass ejections and Forbush decreases. Cosmic rays and Earth, 55-77.

Cane, H.V., Richardson, I.G., Wibberenz, G.: 1995, The response of energetic particles to the presence of ejecta material. Proc. 24th Int. Cosmic Ray Conf.

4, 377.

Chui, C. (Ed.): 1992b, Wavelets: A Tutorial in Theory and Applications. vol. **2**. *Academic Press*, *New York*.

Chui, C.: 1992a, An Introduction to Wavelets. vol. **1**. *Academic Press, New York*.

Daubechies, I.: 1992, Ten Lectures on Wavelets, *CBMS-NSF Regional Conference (Series in Applied Mathematics)*. vol. **61**. SIAM, Philadelphia, PA.

Domingues, M. O., Mendes, O. Jr., & Da Costa, A. M. (2005). On wavelet techniques in atmospheric sciences. Advances in Space Research, 35(5), 831–842. https://doi.org/10.1016/j.asr.2005.02.097

Fagundes, P. R., Cardoso, F. A., Fejer, B. G., Venkatesh, K., Ribeiro, B. A. G., & Pillat, V. G. (2016). Positive and negative GPS-TEC ionospheric storm effects during the extreme space weather event of March 2015 over the Brazilian sector. Journal of Geophysical Research: Space Physics, 121(6), 5613-5625.

Forbush, S. E. (1937). On the effects in cosmic-ray intensity observed during the recent magnetic storm. Physical Review, 51(12), 1108.

Forbush, S. E. (1938). On cosmic-ray effects associated with magnetic storms. Terrestrial Magnetism and Atmospheric Electricity, 43(3), 203-218.

Forbush, S. E. (1954). World-wide cosmic ray variations, 1937–1952. Journal of Geophysical Research, 59(4), 525-542.

Foufoula-Georgiou, E.K., Kumar, P. (Eds.): 1995, Wavelet in Geophysics. *Academic Press, New York*, 373pp.

Gao, R. X., & Yan, R. (2011). From fourier transform to wavelet transform: A historical perspective. In Wavelets (pp. 17-32). Springer, Boston, MA.

Gosling, J. T., McComas, D. J., Phillips, J. L., & Bame, S. J. (1991). Geomagnetic activity associated with Earth passage of interplanetary shock disturbances and coronal mass ejections. Journal of Geophysical Research: Space Physics, 96(A5), 7831-7839.https://doi.org/10.1029/91JA00316

Hess, V. F., & Demmelmair, A. (1937). World-wide effect in cosmic ray intensity, as observed during a recent magnetic storm. Nature, 140(3538), 316-317.

Huang, N. E., Shen, Z., Long, S. R., Wu, M. C., Shih, H. H., Zheng, Q. & Liu, H. H. (1998). The empirical mode decomposition and the Hilbert spectrum for nonlinear and non-stationary time series analysis. Proceedings of the Royal Society of London. Series A: mathematical, physical and engineering sciences, 454(1971), 903-995.

Hubert, G., Pazianotto, M. T., Federico,C. A., & Ricaud, P. (2019). Analysis ofthe Forbush decreases and ground-levelenhancement on September 2017 usingneutron spectrometers operated inAntarctic and midlatitude stations.Journal

of Geophysical Research: SpacePhysics, 124, 661–673. https://doi.org/10.1029/2018JA025834

Ifedili, S. O. (2004), The two-step Forbush decrease: An empirical model, J. Geophys. Res., 109, A02117,doi:10.1029/2002JA009814.

Ifedili, S.O. Magnetic clouds, cosmic ray decreases, and geomagnetic storms. Earth Planet Sp 58, 659–666 (2006). https://doi.org/10.1186/BF03351963

Jin, S., Jin, R. & Kutoglu, H. Positive and negative ionospheric responses to the March 2015 geomagnetic storm from BDS observations. J Geod 91, 613–626 (2017). https://doi.org/10.1007/s00190-016-0988-4

Joselyn, J.A.: 1986, Proceedings of Chapmaan conference on solar wind magnetosphere coupling, edited by F. Kamide and J. A. Slavin Terra Sci. Tokyo, 127.

Kandemir, G., Geçkinli, M., Firat, C., Yilmaz, M., & Ozugur, B. (2002). Cosmic ray intensity variation during a CME. Planetary and Space Science, 50(5-6), 633–636. doi:10.1016/s0032-0633(02)00043-0

Kane, R. P.: 1977, A comparative study of geomagnetic, interplanetary, and cosmic ray storms. Journal of Geophysical Research. 82(4), 561–577. doi:10.1029/ja082i004p00561

Kane, R. P.: Severe geomagnetic storms and Forbush decreases: interplanetary relationships reexamined, Ann. Geophys., 28, 479–489, https://doi.org/10.5194/angeo-28-479-2010, 2010.

Karttunen, H., Kröger, P., Oja, H., Poutanen, M., & Donner, K. J. (Eds.). (2007). Fundamental astronomy (Vol. 4). Berlin: Springer.

Kharayat, H., Prasad, L. Study of cosmic ray intensity and geomagnetic storms with solar wind parameters during the period 1998–2005. Astrophys Space Sci 362, 20 (2017). https://doi.org/10.1007/s10509-016-2996-5

Klausner, V., O. Mendes, M. O. Domingues, A. R. R. Papa, R. H. Tyler, P. Frick, and E. A. Kherani (2014), Advantage of wavelet technique to highlight the observed geomagnetic perturbations linked to the Chilean tsunami (2010), J. Geophys. Res. Space Physics, 119, 3077–3093, doi:10.1002/2013JA019398

Kravtsova, M.V., Sdobnov, V.E. Analyzing the June 2015 Forbush effect by the spectrographic global survey. Bull. Russ. Acad. Sci. Phys. 81, 177–179 (2017). https://doi.org/10.3103/S1062873817020253

Kumar, S., Veenadhari, B., Tulasi Ram, S., Selvakumaran, R., Mukherjee, S., Singh, R., & Kadam, B. D. (2015). Estimation of interplanetary electric field conditions for historical geomagnetic storms. Journal of Geophysical Research: Space Physics, 120(9), 7307-7317.https://doi.org/10.1002/2015JA021661

Le Roux, J. A., & Potgieter, M. S. (1991). The simulation of Forbush decreases

with time-dependent cosmic-ray modulation models of varying complexity. Astronomy and Astrophysics, 243, 531-545.

Lingri, D., Mavromichalaki, H., Belov, A. et al. Solar Activity Parameters and Associated Forbush Decreases During the Minimum Between Cycles 23 and 24 and the Ascending Phase of Cycle 24. Sol Phys 291, 1025–1041 (2016). https://doi.org/10.1007/s11207-016-0863-8

Liu, J., W. Wang, A. Burns, X. Yue, S. Zhang,Y. Zhang, and C. Huang (2016), Profiles of ionospheric storm-enhanced density during the 17 March 2015 great storm,J. Geophys. Res. Space Physics, 121,727–744, doi:10.1002/2015JA021832.

Liu, Y. D., Hu, H., Wang, R., Yang, Z., Zhu, B., Liu, Y. A., & Richardson, J. D. (2015). Plasma and magnetic field characteristics of solar coronal mass ejections in relation to geomagnetic storm intensity and variability. The Astrophysical Journal Letters, 809(2), L34.

Lockwood, J.: 1971, Forbush decreases in the cosmic radiation. Space Science Reviews. 12(5). doi:10.1007/bf00173346.

Mathpal, C., Prasad, L., Pokharia, M., & Bhoj, C.: 2018, Study of cosmic ray intensity in relation to the interplanetary magnetic field and geomagnetic storms for solar cycle 24. Astrophysics and Space Science, 363(8). doi:10.1007/s10509-018-3390-2.

Mendes, O., Domingues, M.O., da Costa, A.M., & Clúa de Gonzalez, A.L.: 2005, Wavelet analysis applied to magnetograms: Singularity detections related to geomagnetic storms. *Journal of Atmospheric and Solar-Terrestrial Physics*. **67**(17-18), 1827–1836. doi: 10.1016/j.jastp.2005.07.004.

Menke, W., & Menke, J. (2012). Environmental data analysis with MatLab. Pages 1-15, ISBN 9780123918864, Academic Press. https://doi.org/10.1016/B978-0-12-391886-4.00001-5.

Meyer, Y. (1990). Ondelettes, filtres miroirs en quadrature et traitement numerique de l'image. Les Ondelettes en, 1989, 14–25. https://doi.org/10.1007/BFb0083512

Mosna, Z., Kouba, D., Knizova, P. K., Buresova, D., Chum, J., Sindelarova, T., ... & Saxonbergova–Jankovicova, D. (2020). Ionospheric storm of September 2017 observed at ionospheric station Pruhonice, the Czech Republic. Advances in Space Research, 65(1), 115-128. https://doi.org/10.1016/j.asr.2019.09.024.

Nayak, C., Tsai, L. C., Su, S. Y., Galkin, I. A., Tan, A. T. K., Nofri, E., & Jamjareegulgarn, P. (2016). Peculiar features of the low-latitude and midlatitude ionospheric response to the St. Patrick's Day geomagnetic storm of 17 March 2015. Journal of Geophysical Research: Space Physics, 121(8), 7941-7960. https://doi.org/10.1002/2016JA022489

P. K. Shrivastava, Proceedings of the 29th International Cosmic Ray Conference. August 3-10, Pune, India 1, 355 (2005).

Ramsingh, S. Sripathi, S. Sreekumar, S. Banola, K. Emperumal, P. Tiwari, andRuskai, M.B., Beylkin, G., Coifman, R., Daubechies, I., Mallat, S., Meyer, Y., Raphael, L. (Eds.): 1992, Wavelets and their Applications, Jones and Bartlett, Boston, MA.

Ramsingh, Sripathi, S., Sreekumar, S., Banola, S., Emperumal, K., Tiwari, P., Kumar, B.S., 2015. Low-latitude ionosphere response to super geomagnetic storm of 17/18 March 2015: results from a chain of ground-based observations over Indian sector. J. Geophys. Res. http://dx.doi.org/10.1002/2015JA021509.

Samara, E., Smponias, A., Lytrosyngounis, I. et al. Unusual Cosmic Ray Variations During the Forbush Decreases of June 2015. Sol Phys 293, 67 (2018). https://doi.org/10.1007/s11207-018-1290-9

Simpson, J. A. (1954). Cosmic-radiation intensity-time variations and their origin. III. The origin of 27-day variations. Physical Review, 94(2), 426.

Singh, P. K., Tripathi, L., Singh, A., Tiwari, J., & Tiwari, A. K. (2008). Solar wind streams and their impact on cosmic ray intensity decreases in year 2003. Rom. J. Phys, 53(7-8), 917-924.

Souza, A. M., Echer, E., Bolzan, M. J. A., & Hajra, R. (2016). A study on the main periodicities in interplanetary magnetic field Bz component and geomagnetic AE index during HILDCAA events using wavelet analysis. Journal of Atmospheric and Solar-Terrestrial Physics,149, 81–86. https://doi.org/10.1016/j.jastp.2016.09.006

Strang, G. (1993). Wavelet transforms versus Fourier transforms. Bulletin of the American Mathematical Society, 28(2), 288-305.

Strang, G., Nguyen, T.: 1996, Wavelet and Filters Bank, Wellesley-Cambridge, Cambridge.

Svensmark, H. (2006). Cosmic rays and the biosphere over 4 billion years. Astronomische Nachrichten: Astronomical Notes, 327(9), 871-875.https://doi.org/10.1002/asna.200610651

Torrence, C., & Compo, G. P. (1998). A practical guide to wavelet analysis. Bulletin of the American Meteorological Society, 79(1), 61–78. https://doi.org/10.1175/1520-0477(1998)079%3c0061:APGTWA%3e2.0.CO;2

Usoskin, I. G., I. Braun, O. G. Gladysheva, J. R. Ho¨randel, T. Ja¨mse´n, G. A. Kovaltsov, and S. A. Starodubtsev (2008),Forbush decreases of cosmic rays: Energy dependence of the recovery phase, J. Geophys. Res., 113, A07102,doi:10.1029/2007JA012955

.

Wanliss, J. A., and K. M. Showalter (2006), High-resolution global storm index: Dst versus SYM-H, J. Geophys. Res., 111,A02202, doi:10.1029/2005JA011034.

Zhao, L. L., & Zhang, H. (2016). Transient galactic cosmic-ray modulation during solar cycle 24: A comparative study of two prominent Forbush decrease events. The Astrophysical Journal, 827(1), 13.DOI:https://doi.org/10.3847/0004-637X/827/1/13

Zhao, L. L., & Zhang, H.: 2016, Transient Galactic Cosmic-Ray Modulation During Solar Cycle 24: A Comparative Study of Two Prominent Forbush Decrease Events. The Astrophysical Journal. 827(1), 13. doi:10.3847/0004-637x/827/1/13.